Chapter 2

Fluid description of shock phenomena in gases and plasmas: a bird's eye view

In the present Chapter we introduce the general subject of this dissertation in an intuitive way. We discuss the concepts, ideas, techniques and terminology that are used to describe shock phenomena in fluids. We give an overview of the results on MHD bow shock flows which are presented throughout this dissertation. We introduce MHD shock phenomena in nature for which the simulation results are relevant.

We believe that it is important to attempt to give such a global overview of the results and their relevance in a single Chapter, which should be easily accessible. In doing so, we touch upon a great variety of often quite complicated subjects, such that our discussion cannot always be rigorous and complete, but necessarily has to remain intuitive at places. Such an intuitive introduction makes the results more easily accessible for the reader who is not so familiar with the topics addressed, while at the same time the more knowledgeable reader may appreciate being reminded of some basic aspects of the physics of shocks and space plasmas. Most of the material covered in this introductory Chapter is discussed more rigorously and completely in the following Chapters. Other topics are not revisited after their brief introduction in the present Chapter, in which case the reader is referred to the literature for more extensive information.

2.1 Hydrodynamic description of shock phenomena in gases

This dissertation deals with shock phenomena in MHD plasmas, which describe *ionized* gases. The dynamical behavior of a *neutral* gas already exhibits many phenomena which are of interest to us. Therefore we introduce some aspects of the fluid dynamics of neutral gases before turning our attention to MHD plasma phenomena.

Although gases consist of free particles which interact through collisions, it is for many purposes sufficient to give a mathematical description of a gas as a continuous fluid. Such a description is given by the hydrodynamic (HD) equations [20, 160, 90, 54]

$$\frac{\partial}{\partial t}\begin{bmatrix}\rho\\ \rho\,\vec{v}\\ e\end{bmatrix}+\nabla\cdot\begin{bmatrix}\rho\,\vec{v}\\ \rho\,\vec{v}\vec{v}+\mathsf{I}p\\ (e+p)\,\vec{v}\end{bmatrix}=\nabla\cdot(\mathsf{D}). \tag{2.1}$$

These equations are formulated in terms of the macroscopic thermodynamic quantities pressure p, mass density ρ and specific total energy e, and in terms of the bulk velocity $\vec{v}$. I is the unity matrix. These equations describe the conservation of mass, momentum and energy. The specific total energy e is given by

$$e=e_{int}+\rho\,\frac{\vec{v}\cdot\vec{v}}{2}, \tag{2.2}$$

with e_{int} the specific internal energy of the gas. The internal energy, the pressure, and the density are related by an equation of state. In this dissertation we assume ideal gas behavior for simplicity, such that (in suitable units)

$$e_{int}=\frac{p}{\gamma-1}\quad\text{and}\quad T=\frac{p}{\rho}, \tag{2.3}$$

where T is the temperature and γ is the adiabatic index. The ideal gas law is a good approximation for most space and solar plasmas. The tensorial quantity D in Eq. 2.1 represents the contribution from irreversible dissipative processes like viscosity and thermal conduction. The matrix of dissipative fluxes D depends on dissipative parameters like the viscosity, and on the state variables and gradients of the state variables. An ideal or dissipationless fluid is described by Eq. 2.1 with $\mathsf{D}\equiv 0$, in which case Eqs. 2.1 are called the Euler equations. When dissipative effects are included the equations are called the Navier-Stokes equations. Most real gasses have a finite dissipation, but this dissipation is often small. It can be neglected for many phenomena, in which case the ideal equations give a good approximate description of the behavior of the real gas.

The Euler equations (Eq. 2.1 with $\mathsf{D} \equiv 0$) allow for sound waves [20, 160, 90, 54], which for small amplitudes are linear perturbations propagating isotropically with the sound velocity

$$c = \sqrt{\frac{\gamma p}{\rho}}. \tag{2.4}$$

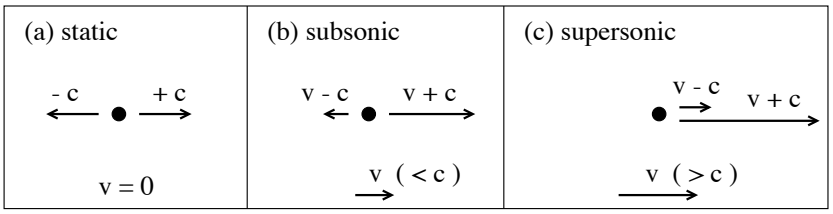

Figure 2.1: *A fixed point source sends out small-amplitude perturbations while a uniform fluid flows along the source with constant velocity v relative to the fixed source. In the frame of the moving fluid, the perturbations propagate to the left and to the right with the wave velocity c. In the frame of the source, the waves are carried by the fluid and propagate with velocities $v - c$ and $v + c$.*

Fig. 2.1 shows schematically how a small-amplitude perturbation generated by a fixed source would propagate in a hypothetical 1D system with uniform background flow. In the static case ($v = 0$), the perturbation propagates to the left and to the right with speeds $-c$ and $+c$ (a negative sign thus means propagation to the left). If there is a uniform background flow to the right with velocity $v < c$, then we say that the flow is *subsonic*. The perturbation can still propagate to the left and to the right with speeds $v - c$ and $v + c$, but $v - c$ now has a smaller magnitude than $v + c$. When the flow is *supersonic* ($v > c$), the perturbation can only propagate to the right, with speeds $v - c$ and $v + c$ both pointing rightwards. This means that in supersonic flow, information cannot propagate in the upstream direction. The sonic Mach number, which is defined as the ratio of the magnitude of the velocity vector and the sound speed

$$M = \frac{||\vec{v}||}{c}, \tag{2.5}$$

is greater than 1 for supersonic flow.

The HD equations 2.1 are *nonlinear*, which can cause large-amplitude waves (Fig. 2.2a) to steepen into shocks (Figs. 2.2b and c). The state variables jump discontinuously at shocks. For the Navier-Stokes equations, the steep shock profile actually remains smooth and the width of

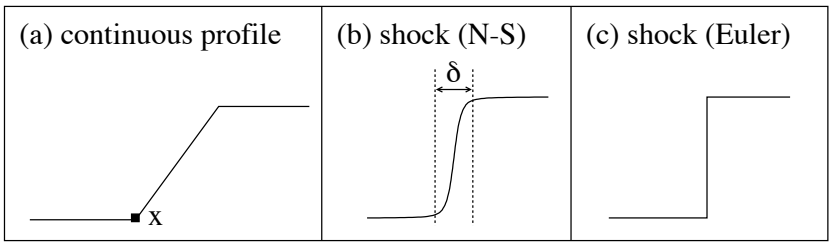

Figure 2.2: *Nonlinear steepening of a large-amplitude profile — for instance the density — into a shock.*

the shock layer δ is related to the values of the dissipative coefficients. The Euler equations, however, allow for strictly discontinuous shock solutions. Strictly speaking, a discontinuous profile cannot be a solution of the partial differential equation (PDE) 2.1, because derivatives are not defined at discontinuities. Discontinuous profiles, however, can be solutions of the *integral* form of the Euler equations, and in this case it is said that they are *weak* solutions of the PDE [90].

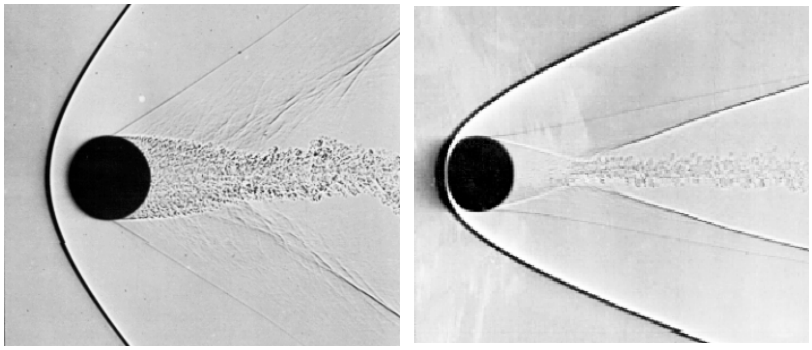

Figure 2.3: *Experimental shadowgraph pictures of a sphere in free flight through air at M=1.53 (left) and M=4.01 (right). (from* An Album of Fluid Motion*, M. Van Dyke [30])*

Fig. 2.3 shows shadowgraph pictures of an experiment where a small sphere flies freely through air (towards the left) with supersonic speeds ($M = 1.53$ and $M = 4.01$) [30]. The flow pattern around the sphere in the left panel of Fig. 2.3 shows several interesting phenomena. The sphere is preceded, on the left, by a paraboloid-like-shaped nearly stationary dark surface, which indicates a sudden jump in density. This surface is a shock surface, and is called a *bow shock*.

We can understand intuitively why this bow shock has to be present. First, let us set our mind on the coordinate system which moves to the left together with the sphere. In this frame, the sphere and the bow shock are nearly *stationary* or *steady*, which facilitates the analysis. In this frame, the gas to the left of the bow shock is no longer at rest, but moves to the right in the direction of the sphere with supersonic speed v. In this supersonic region to the left of the bow shock, information can only propagate to the right, as illustrated in Fig. 2.1c. However, the sphere has to be able to 'communicate' its presence to the flow in front of it, such that the flow field can adapt to the presence of the sphere. This requires that a *subsonic* region forms in the immediate front of the sphere, in which the sphere can make its presence felt through waves capable of propagating to the left (Fig. 2.1b). The flow far upstream (left) remains supersonic, and the subsonic region close to the sphere is connected to the supersonic region upstream by a shock surface. Conceptually, it is not immediately evident why the subsonic region close to the sphere and the supersonic region upstream necessarily have to be connected by a shock. One could imagine that the uniform supersonic upstream region could be connected to the subsonic region by a continuous profile, like in Fig. 2.2a, but stationary in the frame of the sphere. Intuitively one could say that such a continuous profile separating the two regions would steepen into a shock because of nonlinear effects, like in Fig. 2.2. A more sophisticated argument is the following. The small-amplitude perturbation at point x in Fig. 2.2a, where the uniform region would be connected to the slope, would have to move with the local small-amplitude wave speed $v - c$, which is determined by the sound speed c and the velocity v of the incoming supersonic flow. This observation shows that such a configuration can never be stationary in the frame of the sphere, because for supersonic flow $v > c$, and thus $v - c \neq 0$. The uniform supersonic region upstream thus necessarily has to be connected to the subsonic region close to the sphere by a *discontinuous profile* or shock, and analysis shows indeed that a shock can have a *shock speed* which exactly makes the shock stationary in the frame of the sphere.

At the backside of the sphere in the left panel of Fig. 2.3 we see several other structures. A *boundary layer* [160] separates from the sphere, and the flow is highly turbulent (and thus non-stationary) in the resulting wake. An additional shock can be seen where the boundary layer separates, both on the top and the bottom of the sphere in the figure. The $M = 4.01$ flow (right panel of Fig. 2.3) shows similar features as the $M = 1.53$ flow.

It is thus clear that shock phenomena in gases are quite complex. The HD equations offer an adequate description of many of these phenomena, but, mainly due to the inherent nonlinearity of the equations, it is hard to find explicit analytical solutions for 2D and 3D flow problems.

Therefore, the alternative to solve the HD equations using numerical methods on computers has proven to be a useful approach. When geometries are modeled accurately and parameter values are chosen with care, numerical simulations of Euler or Navier-Stokes flows around geometrically complex objects agree well with experiments [167]. Numerical simulations are especially useful to study physical phenomena in regimes of parameters and physical sizes for which experiments cannot reasonably be performed, and for which detailed observations are not available. It would seem that this applies to many phenomena in space physics and astrophysics.

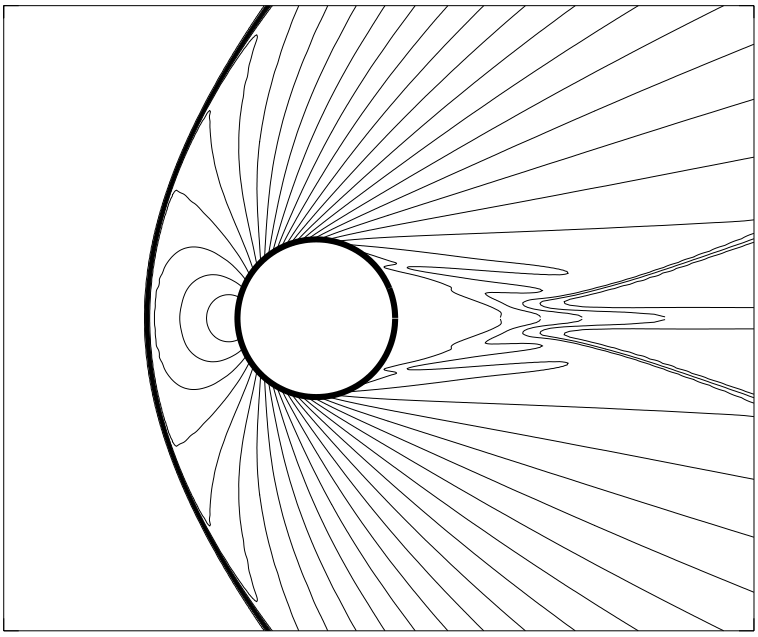

Figure 2.4: *Numerical simulation of supersonic hydrodynamic flow around a cylinder (thick solid). The flow comes in from the left ($M = 2.6$). Density contours (thin solid) pile up in shocks.*

In Fig. 2.4 we show numerical simulation results for the $M = 2.6$ flow of a gas around a cylinder. These simulations were performed with our numerical simulation code, which discretizes the ideal HD equations but introduces a small amount of numerical dissipation. Contours of equal density are shown. In this simulation we did not attempt to faithfully model the geometry and parameter regime of the experimental flows

of Fig. 2.3, but we want to demonstrate in a qualitative way that the simulation results reproduce many of the flow features present in the experiments. The density contours pile up in a stationary bow shock on the left of the cylinder. Boundary layers separate from the back of the cylinder. The spatial resolution of the simulation is not high enough, however, to reproduce turbulence in the wake [167].

In this dissertation, we study stationary bow shock configurations around cylinders and spheres, much like the configurations in Figs. 2.3 and 2.4, using numerical simulation techniques. Most of the time we focus on the bow shock itself. This allows us to limit the simulation to the half-plane on the upstream side of the center of the cylinder or the sphere. We then expect a resulting flow which is in a perfect non-turbulent steady state. We are, however, not concerned with flows in non-conducting fluids which describe neutral gases, but on the contrary we are interested in bow shock flows in MHD plasmas which model *ionized* gases. Much of the discussion on neutral gas dynamics that was given above, remains relevant for plasma flows. The fact that plasma particles are charged and MHD plasmas thus conduct currents, however, introduces interesting additional dynamical effects, which are discussed next.

2.2 Magnetohydrodynamic description of shock phenomena in plasmas

At sufficiently high temperatures, the atoms or molecules in a gas lose negatively charged electrons and thus become positively charged ions themselves. Such a gas of charged particles is called a plasma.

A continuous fluid description of a plasma is given by the magnetohydrodynamic (MHD) equations [87, 118, 7, 54]. We now briefly introduce the MHD equations and the properties of MHD waves and shocks. A more complete discussion is given in Chap. 3. The MHD equations read in conservation form

$$\frac{\partial}{\partial t}\begin{bmatrix} \rho \\ \rho\,\vec{v} \\ \vec{B} \\ e \end{bmatrix} + \nabla\cdot\begin{bmatrix} \rho\,\vec{v} \\ \rho\,\vec{v}\vec{v} + \mathsf{I}\left(p + \vec{B}\cdot\vec{B}/2\right) - \vec{B}\vec{B} \\ \vec{v}\vec{B} - \vec{B}\vec{v} \\ \left(e + p + \vec{B}\cdot\vec{B}/2\right)\vec{v} - \left(\vec{v}\cdot\vec{B}\right)\vec{B} \end{bmatrix} = \nabla\cdot(\mathsf{D}) - \begin{bmatrix} 0 \\ \vec{B} \\ \vec{v} \\ \vec{v}\cdot\vec{B} \end{bmatrix}\nabla\cdot\vec{B}. \qquad (2.6)$$

$\vec{B}$ is the magnetic field, with units chosen such that the magnetic permeability $\mu = 1$. This equation has to be supplemented with the divergence free condition $\nabla \cdot \vec{B} = 0$ as an initial condition. The second right hand side term of Eq. 2.6 is proportional to $\nabla \cdot \vec{B} = 0$ and is thus equal to zero. For several reasons to be explained further on, it is advantageous to keep this term in the equations. The total specific energy is given by

$$e = \frac{p}{\gamma - 1} + \rho \frac{\vec{v} \cdot \vec{v}}{2} + \frac{\vec{B} \cdot \vec{B}}{2}. \tag{2.7}$$

For the dissipative MHD equations, the matrix of dissipative fluxes D depends on dissipative parameters like the viscosity and the electric resistivity, and on the state variables and gradients of the state variables. The ideal MHD equations describe a dissipationless conducting fluid, and are given by Eq. 2.6 with $\mathsf{D} \equiv 0$. The MHD equations describe the conservation of mass, momentum, magnetic field, and energy.

Inspection of Eq. 2.6 shows that the magnetic field influences the velocity of the plasma — through the $\vec{J} \times \vec{B}$ force, with $\vec{J} = \nabla \times \vec{B}$ — and that the magnetic field in its turn is influenced by the moving fluid. These effects result in a dynamical behavior which is quite more complicated than in the case of a non-conducting fluid. MHD allows for *three* different linear wave modes, the fast magnetosonic, the Alfvén, and the slow magnetosonic wave [87, 54]. Due to the extra $\vec{J} \times \vec{B}$ force in the momentum equation, which depends on the magnetic field and its direction, the three linear wave speeds become strongly dependent on the direction relative to the local magnetic field. It is said that MHD waves are *anisotropic*. The fact to be illustrated below that MHD bow shock flows can exhibit much more complex behavior than their HD counterparts can be related to this anisotropy. The fast, Alfvén (or intermediate) and slow wave speeds in the direction x are represented by c_{fx}, c_{Ax} and c_{sx}, respectively. The Alfvén speed is given by $c_{Ax} = |B_x|/\sqrt{\rho}$. For any direction x, it holds that $c_{fx} \geq c_{Ax} \geq c_{sx}$. In the direction of the magnetic field, the fast wave speed coincides with the largest of the sound and the Alfvén speed, while the slow wave speed coincides with the smallest of the two. Slow waves and Alfvén waves have a vanishing propagation speed in the direction perpendicular to the magnetic field.

Due to nonlinear effects large-amplitude MHD waves can steepen into shocks [4, 87, 80]. There exist three different types of MHD shocks, as shown in Fig. 2.5, and we can distinguish between them by considering the way in which they refract the magnetic field. Fast MHD shocks refract the magnetic field away from the shock normal (Fig. 2.5a), such that the upstream angle between the shock normal and the magnetic field θ_1 is smaller than the downstream angle θ_2 (in Fig. 2.5 the plasma flow in the shock frame goes from left to right). In an intermediate MHD

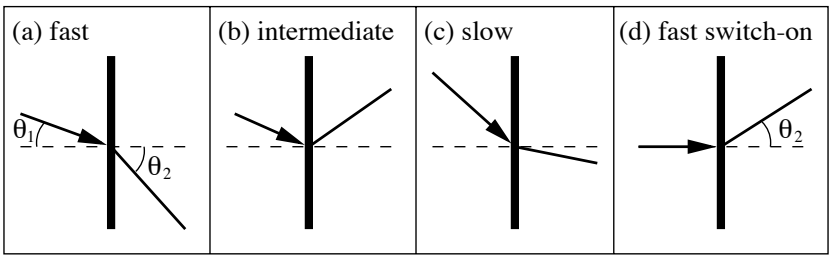

Figure 2.5: *MHD shock types. The magnetic field (arrowed) is refracted at the shock (thick). The shock normal is dashed. Region 1 is upstream, 2 is downstream.*

shock the magnetic field line is flipped over the shock normal (Fig. 2.5b). Slow MHD shocks refract the magnetic field toward the shock normal (Fig. 2.5c).

In Fig. 2.5d we show the peculiar MHD shock phenomenon which is called a fast switch-on shock. The upstream magnetic field is perpendicular to the shock front, but downstream there exists a finite angle θ_2 between the shock normal and the magnetic field.

Switch-on shocks have no analog in the hydrodynamic flow of a neutral fluid, and can thus be called an intrinsically magnetic effect. Switch-on shocks can occur when the inflow plasma β, which is defined as the ratio of the thermal pressure to the magnetic pressure ($\beta \equiv p/(B^2/2)$), is smaller than $2/\gamma = 1.2$, and when, along the magnetic field lines, the incoming plasma velocity lies between the fast MHD wave speed and roughly twice this speed [80]. This parameter regime is called the *switch-on regime*. Switch-on shocks thus arise when magnetic forces dominate over thermal pressure and dynamic pressure effects. Switch-on shocks occur when the upstream magnetic field is strong and are an intrinsically magnetic effect. Therefore we call upstream flows for which switch-on shocks occur *magnetically dominated* flows. Upstream flows for which switch-on shocks do not occur are called *pressure-dominated* flows.

It is clear that, analogous to the HD case, the formation of a bow shock can be expected when MHD flows fall in on blunt bodies with a velocity which is faster than the fast MHD wave speed — in which case we say that the flow is *superfast*. We may, however, expect additional phenomena due to the influence of the magnetic field and the more complex nature of the MHD equations. It turns out that for magnetically dominated upstream flows MHD bow shocks exhibit a new complex topology which is very different from the traditional topology obtained for bow shocks with pressure-dominated upstream flows. This motivates the introduction of the terminology of pressure-dominated versus magnetically

dominated upstream flows as defined above, and warrants its extension to pressure-dominated versus magnetically dominated bow shock flows and bow shock flow topologies.

In this dissertation we discuss numerical simulation results of MHD bow shock flows around perfectly conducting cylinders and spheres. Our numerical code discretizes the ideal MHD equations, but introduces a small numerical dissipation. The numerical solutions thus describe MHD plasma flows with small dissipation. In the following Sections we give a preview of the results and the phenomena encountered.

A note on notation for wave speeds and Mach numbers

MHD wave speeds and Mach numbers — defined as the ratios of plasma velocities and wave speeds for the various waves — are anisotropic, so we have to define clearly how we refer to them. In general, we specify the direction in which we take wave speeds and Mach numbers in the subscript of the referring symbols, except for scalar quantities which do not depend on the direction. Thus c_{fx}, c_{Ax} and c_{sx} represent the (positive) MHD wave speeds in the direction x. The (positive) sound speed c is isotropic. Sometimes the Alfvén speed in the direction of the magnetic field is referred to as *the* Alfvén speed (or the total Alfvén speed), which we then represent as $c_A = ||\vec{B}||/\sqrt{\rho}$, without subscript x, and with $||\vec{B}||$ the magnitude of the magnetic field vector. $M_{fx} = |v_x|/c_{fx}$, $M_{Ax} = |v_x|/c_{Ax}$ and $M_{sx} = |v_x|/c_{sx}$ are the fast, intermediate and slow Mach numbers, respectively, with $|v_x|$ the absolute value of the plasma velocity in direction x. The sonic or acoustic Mach number in the direction x is given by $M_x = |v_x|/c$. Sometimes the sonic Mach number in the direction of the velocity is referred to as *the* Mach number (or the total Mach number), which we then represent as M, without subscript x. This quantity is thus defined as $M = ||\vec{v}||/c$, with $||\vec{v}||$ the magnitude of the velocity vector. When the magnetic field is everywhere aligned to the plasma velocity — we call this *field-aligned flow* —, the Alfvénic Mach number becomes independent of the direction, in which case we drop the subscript x. The Alfvénic Mach number is then defined as $M_A = ||\vec{v}||/c_A$.

2.2.1 Symmetrical two-dimensional flow around a cylinder

First we treat the 2D problem of uniform flow falling in on a cylinder. We basically take the configuration of Fig. 2.4, but initially we prefer to reduce the complexity of the problem as much as possible. We concentrate on the bow shock, such that the simulation domain can be restricted to the left half plane (the flow comes in horizontally from the left). We also

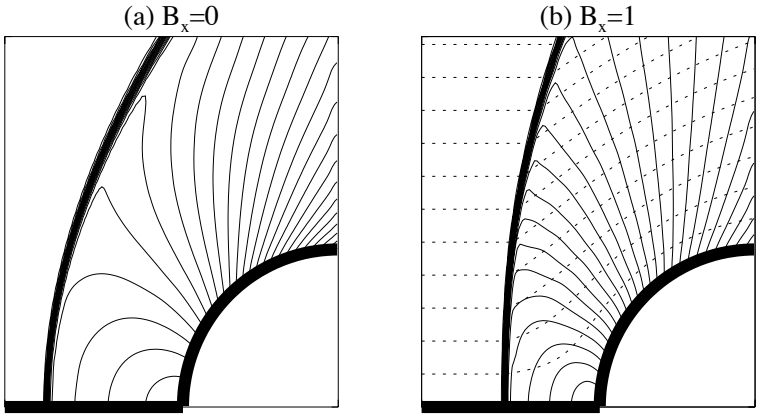

Figure 2.6: *Symmetrical bow shock flows around a cylinder (thick solid). The flow comes in horizontally from the left. Density contours (thin solid) pile up in the bow shock. Magnetic field lines are dotted. The thick solid horizontal line is a line of symmetry. (a) Hydrodynamic flow:* $B_x = 0$, $M = 3.46$. *(b) Pressure-dominated MHD flow:* $B_x = 1$, $M = 3.46$, $M_A = 2$, $\beta = 0.4$.

exploit the symmetry of the problem, by realizing that the horizontal line coming in from the left and going through the center of the cylinder is a line of top-bottom symmetry. This line is called the *stagnation line* because a *stagnation point* — a point with vanishing flow velocity — exists at the intersection of this line with the cylinder. This symmetry allows us to carry out the simulation in the upper left quadrant only. The simulation result for a $M = 3.46$ HD bow shock flow ($\vec{B} = 0$) is shown in Fig. 2.6a. On the stagnation line we explicitly impose symmetry boundary conditions. This flow can thus also be considered as the flow over a plate with a semi-circular bump or corner. It will turn out later that this may be an important detail for stability reasons, so we repeat that we explicitly impose the top-bottom symmetry in these bow shock flows around cylinders, and we call the bow shock flows *symmetrical*. The resulting stationary HD bow shock flow of Fig. 2.6a shows the expected bow shock geometry, with a bow shock which is curved *concave-inward* (towards the cylinder), like the bow shocks in the experimental results of Fig. 2.3.

In Fig. 2.6b we have added a horizontal magnetic field in the inflowing plasma, parallel to the incoming velocity. It can be proved theoretically that the upstream magnetic field has to be taken parallel to the flow

velocity in order to obtain a steady flow solution, and that the magnetic field is then parallel to the plasma velocity in the whole bow shock solution — the flow is thus field-aligned. The sonic Mach number of the inflow is still $M = 3.46$, and the Alfvénic Mach number $M_A = 2$. The plasma β equals 0.4. Switch-on shocks cannot arise for these parameter values, so we call the upstream flow pressure-dominated. The flow is superfast, and we expect a bow shock in front of the cylinder in the stationary simulation result. This bow shock can indeed be seen in Fig. 2.6b. The magnetic field has changed the shape of the bow shock a little compared to the case with $\vec{B} = 0$, but the concave-inward bow shock orientation is preserved. The bow shock is of the fast type along the entire shock surface, because the magnetic field lines (dotted) are refracted away from the shock normal. For this pressure-dominated flow we find the same bow shock flow topology as for the hydrodynamic bow shock flow of Fig. 2.6a. We can say that the hydrodynamic bow shock flow is also pressure-dominated because $\vec{B} \equiv 0$.

Fig. 2.7 shows the simulation result of a MHD bow shock flow with upstream conditions $M = 2.6$, $M_A = 1.5$ and $\beta = 0.4$. Switch-on shocks can arise for these parameter values, so we call the upstream flow magnetically dominated. The topology of the flow is surprisingly different from the topology of the flow in Fig. 2.6b. A switch-on shock occurs at the point well above the stagnation line where the magnetic field is perpendicular to the leading shock front. We see that the central part of the bow shock is now oriented *concave-outward* (away from the cylinder). This feature has been observed first by Steinolfson and Hundhausen [147] in numerical simulations of time-dependent MHD flows related to solar coronal mass ejections, and they called it a 'dimple' in the shock front. They related this phenomenon to the occurrence of switch-on shocks, and it is indeed remarkable that the flow of Fig. 2.6b, with the 'traditional' bow shock topology, has parameters *outside* the regime in which switch-on shocks are possible, whereas the complicated bow shock of Fig. 2.7 has parameters *inside* the switch-on regime!

A second unusual feature of the flow in Fig. 2.7 is that the leading shock front is followed by several secondary shock fronts, which turn out to be of various MHD shock types, as can already be observed from the intricate way in which the magnetic field lines are refracted by these shocks. These interesting features were not anticipated in Steinolfson and Hundhausen's important earlier work [147].

These results suggest that, depending on the upstream conditions, two entirely different topologies exist for MHD bow shock flows. For magnetically dominated upstream flows — for which switch-on shocks occur —, a complex topology arises involving several interacting shock fronts with segments of various MHD shock types. For pressure-dominated upstream flows the traditional single-front topology known from hy-

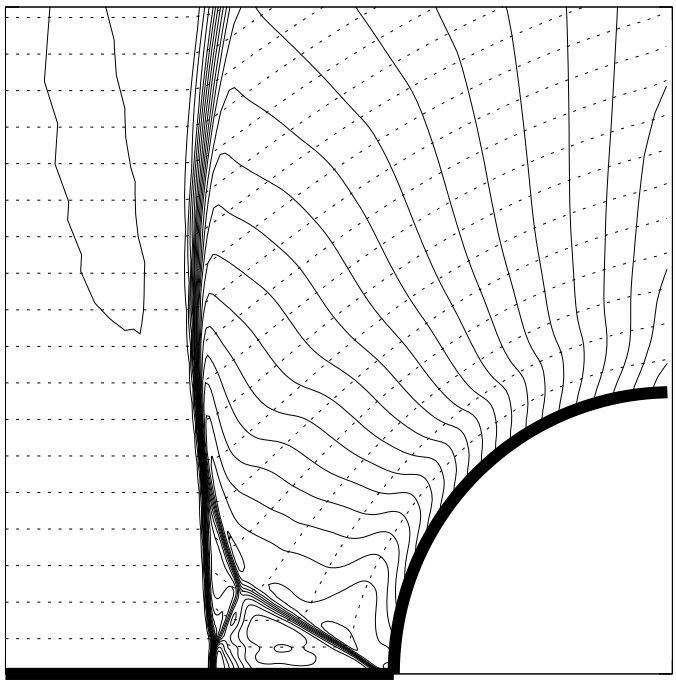

Figure 2.7: *Magnetically dominated MHD bow shock flow:* $B_x = 1$, $M = 2.6$, $M_A = 1.5$, $\beta = 0.4$. *The flow comes in from the left. Density contours (solid) pile up in shocks. Magnetic field lines are dotted. The leading shock front has a concave-outward central part ('dimple'), and is followed by secondary shock fronts.*

drodynamic bow shock flows is recovered. The magnetically dominated bow shock topology of Fig. 2.7 was previously unknown. Its complexity is due to intrinsically magnetic effects.

2D MHD bow shock flows around cylinders are discussed in detail in Chap. 6. We identify and study in detail the nonlinear wave features present in the complex magnetically dominated bow shock flows.

2.2.2 Three-dimensional flow over a sphere

3D MHD bow shock flows are important for space physics applications. The 2D results introduced above suggest that intrinsically magnetic effects may also affect the topology of 3D MHD bow shocks with magnetically dominated upstream flows. We consider stationary 3D bow shock flows over a sphere. In these 3D flows the magnetic field and the plasma velocity do not have to be aligned.

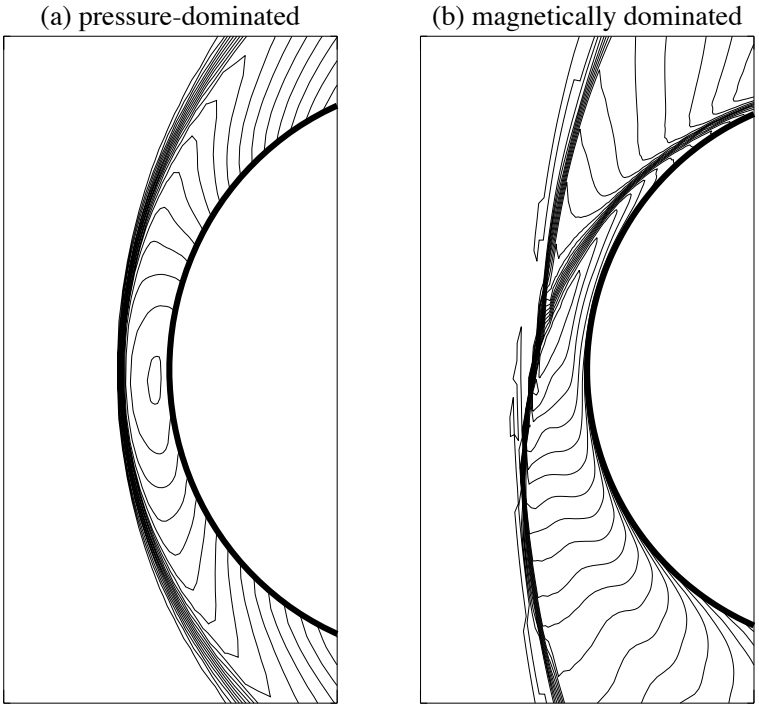

Figure 2.8: *Bow shock flows over a sphere (thick solid) with a small angle between the upstream magnetic field and velocity. The flow comes in from the left. Density contours (thin solid) in a plane through the sphere center are shown. (a) Pressure-dominated flow:* $B_x = 1$, $M_x = 6.90$, $M_{Ax} = 3.985$, $\beta = 0.4$, $v_x = 3.985$, $v_y = 0.022$. *(b) Magnetically dominated flow:* $B_x = 1$, $M_x = 2.6$, $M_{Ax} = 1.5$, $\beta = 0.4$, $v_x = 1.5$, $v_y = 0.01$.

In Fig. 2.8a we show the simulation result of a superfast pressure-dominated MHD flow over a perfectly conducting sphere, with parameters $B_x = 1$, $M_x = 6.90$, $M_{Ax} = 3.985$ and $\beta = 0.4$, and with a small angle between the horizontal magnetic field and the plasma flow ($v_x = 3.985$ and $v_y = 0.022$). Density contours are shown in the plane through the center of the sphere which contains the inflow magnetic and velocity field vectors. We are not surprised to find a stationary solution with a traditional concave-inward (towards the sphere) single shock surface, because the inflow is pressure-dominated.

Let us now investigate the case of a magnetically dominated inflow with parameters $B_x = 1$, $M_x = 2.6$, $M_{Ax} = 1.5$, $\beta = 0.4$, and a small angle between the inflow magnetic field and the velocity ($v_x = 1.5$ and $v_y = 0.01$). Fig. 2.8b shows the steady state solution for this bow shock flow. The existence of a slight dimple and a secondary shock front is confirmed (compare to the 2D flow of Fig. 2.7), and the global bow shock topology of Fig. 2.8b, for magnetically dominated parameters, is very different from the traditional concave-inward single-front bow shock topology of Fig. 2.8a for pressure-dominated parameters. This indicates that intrinsically magnetic effects change the topology of bow shock flows drastically for magnetically dominated upstream parameter values.

Analogous to the 2D case, these results suggest that depending on the upstream conditions, two entirely different topologies exist for 3D MHD bow shock flows. For pressure-dominated upstream flows the traditional single-front topology known from hydrodynamic bow shock flows is recovered. For magnetically dominated upstream flows a previously unknown complex topology arises. This is the main result presented in this dissertation.

Magnetically dominated 3D MHD bow shock flows over spheres are discussed in detail in Chap. 7.

In the next Section we give a brief overview of where MHD bow shocks can be found in nature, and where our findings on magnetically dominated MHD bow shock topology may be relevant.

2.3 MHD shock phenomena in nature

In this section we give an overview of where plasma bow shocks can be encountered in nature, and how these bow shocks have been described in the literature using the MHD model. But first we say something about the validity of the MHD model to describe a plasma, and about the stability of intermediate MHD shocks.

2.3.1 The validity of the MHD approximation

A plasma is a gas composed of charged particles. There exists a hierarchy of theories to describe plasma motion at different levels of complexity (see e.g. [84, 54] for an introduction).

Particle dynamics considers directly the forces exerted on individual particles and the influence of the particles on the electric and magnetic fields (via the *Maxwell equations*). It is obvious that such a description entails a complexity which is often prohibitive, because macroscopic volumes of gas contain an enormous amount of particles. An important consideration is the nature of the physical application at hand, i.e. whether it is necessary to follow the motion of every single particle in order to analyze the behavior of the plasma in the application. Analytical theory is not much developed, but attempts are made to describe particle plasma dynamics using supercomputer simulations.

The *kinetic theory of plasmas* is a statistical theory of plasma motion, which describes the evolution of a *distribution function*. This function represents the number density of particles in function of spatial coordinates, velocity, and time, and is a solution of a *Boltzmann equation*, which needs to be solved together with the Maxwell equations. Some analytical results can be obtained, but the complexity is often prohibitively high, even when numerical approaches are used.

The MHD equations are a continuum fluid description of a plasma, in terms of evolution equations for the macroscopic state variables, and with the Maxwell equations built-in into the formulation. This description, which can be derived by taking moments of the Boltzmann equation, is much more tractable than the particle or kinetic theories, and the mathematical properties of ideal MHD as a symmetrical hyperbolic system [21] are clearly defined. However, one pays a price for this tractability. Many complex dynamical phenomena are retained in the MHD description, but many other microscopic and some macroscopic plasma phenomena are not properly described by the MHD equations.

It is thus important to identify and bear in mind the range of parameters for which the MHD description of a plasma is a good approximation. The ideal MHD equations introduced in Sec. 2.2 describe a fully ionized plasma for which the following properties hold. The particles are considered as *one fluid*, which means that the ions and electrons have to be in thermal equilibrium. A MHD plasma is quasi-neutral, meaning that in a small volume (of the size of a Debeye sphere [54]) positive and negative charges neutralize. The pressure is isotropic. The plasma velocities are non-relativistic. All charged particles gyrate around magnetic field lines with the Larmor frequency ω_L, which is given by

$$\omega_L = \frac{qB}{m}, \tag{2.8}$$

with q the charge of the particle, and m its mass. Ions have a greater mass than electrons, so the gyro-frequency is lower and the gyro-radius is larger for ions than for electrons. This gyration is not retained in the MHD description. MHD is thus valid when the frequencies in the solution are smaller than the ion gyro-frequencies. Also, local length scales in the MHD solution have to be larger than the ion gyro radius. Similarly, MHD frequencies have to be lower than electron plasma frequencies. Electrons are much lighter than ions, such that the inertia and macroscopic velocity of a plasma are mainly due to ions, while the electric current is due to the electron motion relative to the ions. The electric resistivity η can be neglected when the magnetic Reynolds number

$$R_m = \frac{Lv}{\eta}, \tag{2.9}$$

is large, where L is a characteristic length of the problem, and v is a characteristic velocity. If in addition other dissipative mechanisms can be neglected as well, the equations of ideal MHD can be used to describe the plasma behavior. Another important point is that the particle distribution function has to be nearly Maxwellian for the MHD approximation to be valid. In ordinary gases, collisions between particles provide the necessary dissipation to relax the distribution function towards a Maxwellian. In many plasmas in the real world, however, the *mean free path* of plasma particles is much larger than the length scale of the total plasma volume, which means that they hardly undergo any collision. Those plasmas are said to be *collisionless*. But this raises the question which process provides the dissipation in plasmas necessary to relax to Maxwellian states? Or which mechanism provides the dissipation in plasma shocks? Actually, it turns out that most plasmas are not very close to be Maxwellian, and in this sense the MHD description is only an approximation. The shocks formed in collisionless space plasmas dissipate by microscopic particle-wave interactions and instabilities [27, 120].

We have thus to be aware that MHD is only an approximate description of plasma behavior. It is, however, interesting and worthwhile to investigate plasma shock phenomena in the MHD approximation (see e.g. [74] for interesting thoughts on this issue). The MHD equations are statements of the fundamental conservation of mass, momentum, magnetic field and energy, and they often give a good description of plasma phenomena on a macroscopic scale, even if not all microscopic processes are faithfully reproduced in detail. Furthermore, the equations of ideal MHD have a well-defined mathematical structure, and the complexity is tractable. The phenomena that are to be described in this dissertation, are fundamentally 2D and 3D. Plasma particle simulations or kinetic simulations are feasible in 1D, but would require non-trivial computing

resources in 2D and certainly in 3D.

In this dissertation we thus study plasma shocks in the MHD approximation. It is important to understand the behavior of these nonlinear wave phenomena in the MHD system, and the well-defined mathematical nature of the system allows for rigorous analysis of the results and is useful for the development of rigorous numerical methods. We may then expect that our results on MHD bow shocks apply to shocks in real plasmas on a global macroscopic scale, although we are aware that not all plasma phenomena are retained in the MHD description. In the following paragraphs we illustrate how some plasma shock phenomena in space physics have been successfully described in the MHD model. But first we say something about the stability of intermediate shocks.

2.3.2 On the physical existence of intermediate and compound shocks

Intermediate shocks

It has been believed for a long time that intermediate shocks are unphysical [87]. Intermediate shocks were found to be unstable (in a certain peculiar sense, see [87]) in the *ideal* MHD system. Intermediate shocks were said to be 'non-evolutionary', and it was concluded that non-evolutionary shocks cannot exist in nature.

However, recently it has been shown that intermediate shocks can be stable in the *dissipative* MHD system for wide ranges of the dissipation coefficients [173, 43, 49, 110]. They can be destabilized by magnetic perturbations out of the plane formed by the shock normal and the magnetic field (Alfvén waves), but only when the amplitude of the perturbation is sufficiently large [171]. The amplitude of the perturbation required for destabilization decreases with decreasing dissipation [47, 102]. It would seem that dissipative MHD with small dissipation coefficients applies more directly to nature than perfectly ideal MHD. Consequently most authors now seem to agree that intermediate shocks can exist in nature and can persist when perturbations are not too large, although others keep on arguing against the existence of intermediate shocks [35]. In our simulation code we discretize the ideal MHD equations, but numerical dissipation plays a role analogous to a small physical dissipation. We will show that stationary intermediate shock fronts are present in our 2D and 3D MHD simulation results (Figs. 2.7 and 2.8b). This seems to be relevant for the ongoing debate on the physical existence of intermediate shocks. Intermediate shocks have been found before in one-dimensional simulations of the dissipative MHD equations [170], but it seems that our simulations are the first confirmation in 3D that intermediate shocks can indeed exist and persist for small dissipation MHD in a realistic flow configuration.

It is an interesting question what the 3D bow shock solutions with magnetically dominated upstream parameter values would be in some limit of vanishing dissipation [47], or in perfectly ideal MHD. Some authors seem to indicate that for some problems vanishing dissipation limit solutions and the perfectly ideal solution could be different, because small dissipation MHD and ideal MHD do not approach each other uniformly [48, 47] if one considers shock solutions. The precise type and magnitude of the dissipation may influence results to some problems in a non-uniform way. This non-uniform behavior of the vanishing dissipation limit is attributed to the fact that the MHD system is *non-strictly hyperbolic* — wave speeds may coincide — and *non-convex* (see below). The Euler equations are strictly hyperbolic and convex, and the Navier-Stokes equations approach the Euler equations uniformly for vanishing viscosity. This means that Euler simulation codes with numerical diffusion approach the ideal Euler solution to problems uniformly when grids are refined. The above discussion indicates that this may not be true for the MHD case. Some authors reject the use of ideal MHD to describe physical systems precisely because ideal MHD is not a uniquely defined limit of dissipative MHD [173]. However, all these considerations remain speculative because the limit of vanishing dissipation MHD, and the relation between vanishing dissipation MHD and perfectly ideal MHD, have not been understood yet in full [40, 173, 44, 46, 47].

If these considerations on non-uniformity were to be true, however, then the consequence would be that for some problems ideal MHD solutions cannot be calculated with numerical codes which introduce numerical dissipation [48], and that for small dissipation MHD calculations — which presumably would correspond to most physical applications — the dissipative effects should be modeled explicitly, because solutions may depend on the specific form of the dissipation [173]. Most researchers do not seem to be aware of these concerns. Recently many new algorithms have been presented which are intended to solve the ideal MHD equations [12, 157, 158, 183, 23, 128, 1, 118, 162, 6, 7, 99, 36, 26, 111, 5], and when those techniques are applied to space physics and astrophysics flows, it is generally believed that the solutions approach the ideal MHD solution. The above discussion indicates that it would be best to include an explicit description of dissipation mechanisms in numerical MHD simulations. However, this makes numerical MHD codes more complex and demands substantially larger computing resources. Therefore we adopt the pragmatic approach — which is customary in the field of space physics and astrophysics research — of utilizing a numerical code which discretizes the ideal MHD equations, but in which numerical dissipation plays a role analogous to a small physical dissipation. We will then argue that our simulation results are solutions of the MHD equations with small dissipation. This small dissipation remains unspecified, however,

and this is not very satisfactory. It remains thus an interesting topic of future research to verify the bow shock flow solutions which are presented in this dissertation with a numerical code which explicitly models the dissipation mechanisms, and to study vanishing dissipation limits or ideal MHD solutions. As mentioned above, the small dissipation case would seem the most appropriate to describe physical systems. In this sense the discussion on vanishing dissipation limits and ideal MHD solutions is probably not so relevant for space physics applications, although these topics remain interesting mathematical problems. Our simulation results are probably relevant for bow shock flows in space physics and astrophysics flows, because they confirm in 3D that intermediate shocks can indeed exist and persist for small dissipation MHD in a realistic flow configuration.

The problem of the existence of intermediate shocks is very subtle and has probably not been resolved yet in full. Therefore we dedicate a full Chapter (Chap. 9) to the discussion of this topic. We illustrate the main issues of the ongoing debate on the existence of intermediate shocks and we discuss the relevance of our results for this debate.

Compound shocks

MHD compound shocks are intermediate shocks for which the plasma velocity exactly equals the fast or the slow wave speed in the upstream or downstream state of the shock. MHD allows for compound shocks because the MHD system is non-convex [11, 90, 109]. MHD compound shocks were initially believed to be unphysical because they are a special kind of intermediate shock, which was believed to be non-evolutionary. But compound shocks were found in 1D numerical simulations of the MHD equations [12], and they were shown to be necessary elements in the analytical solution of planar MHD Riemann problems [110].

We show in Chapters 6 and 7 of this dissertation that our simulation results of flows around cylinders and spheres (Figs. 2.7 and 2.8b) clearly contain compound shocks. These peculiar nonlinear wave structures were earlier found in 1D simulations, but our results seem to be the first clear confirmation that compound shocks can arise in 2D and 3D flows.

2.3.3 Bow shocks in the solar system: planets, comets and the heliosphere

Nearly stationary plasma bow shock configurations can be found in the solar system where the superfast solar wind [67] encounters planets or comets [84].

Fig. 2.9 shows a sketch of the earth's magnetic environment [168]. The earth has an intrinsic magnetic field, which is confined to a region

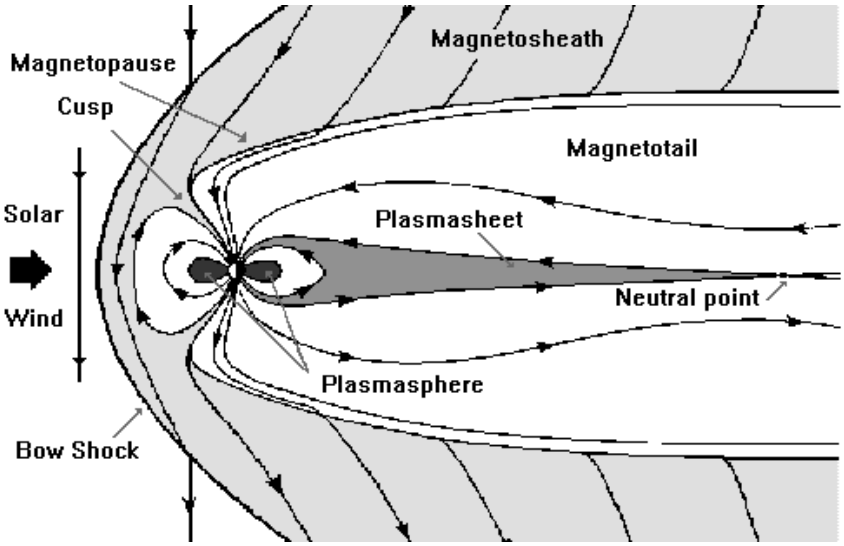

Figure 2.9: *The earth's magnetic environment. (courtesy ISPEC)*

which is called the *magnetosphere*. This region is separated from the solar wind magnetic field by the *magnetopause*. The solar wind flow is deflected to flow around the magnetopause, and this deflection involves a transition through a bow shock from a superfast to a subfast state, as was explained in Sec. 2.1 and as is seen in the MHD simulations of Sec. 2.2. The region between the bow shock and the magnetopause is called the *magnetosheath*.

Fig. 2.10 shows a time series of local magnetic field and electron temperature measurements of the Ulysses spacecraft crossing Jupiter's bow shock [115]. A clear jump in magnetic field and electron temperature can be seen at approximately 17:30 UT, which can be demonstrated to quantitatively agree with a fast MHD shock transition.

All planets are expected to have bow shocks, and this has been proven by direct measurements of passing spacecraft, except for Pluto [143]. Some spacecraft have crossed cometary bow shocks [73]. Such satellite observations are important, because they establish the presence of the bow shocks, but they are limited in the sense that they provide only datasets along a 1D curve. Direct observations of the spatial geometry and extent of planetary bow shocks are not available. The 1D observations do, however, provide us with detailed observations of local shock transitions. These observations show that those planetary and cometary bow shocks are not just 'clean' MHD shock transitions, because wave perturbations are present upstream and downstream of the shocks (Fig.

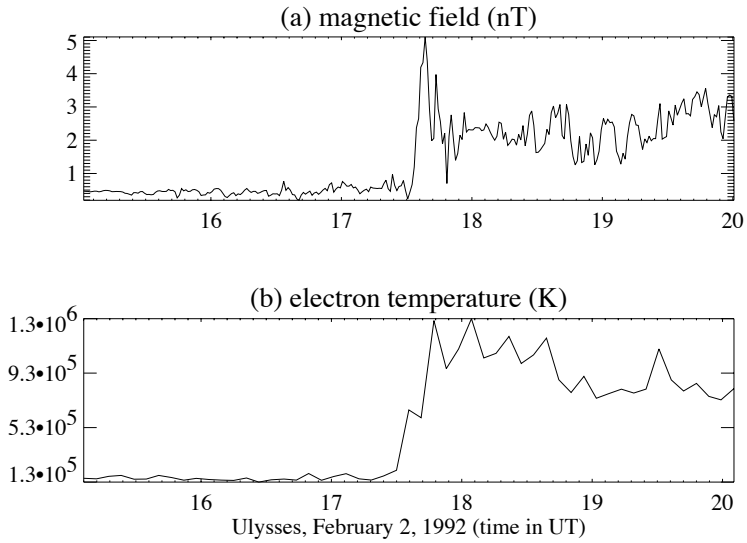

Figure 2.10: *Ulysses crosses Jupiter's bow shock. (courtesy D. Balogh and J. Phillips, NSSDC)*

2.10) and because the shock profiles have structures which indicate that particle and kinetic processes, neglected in the MHD description, are present. Explanations have been proposed for many types of observed wave perturbations and for observed shock structures, based on detailed particle and kinetic plasma models [27].

The global bow shock flows can often be modeled quite satisfactorily using the MHD model, and MHD models have reproduced successfully many aspects of the observations, for flows around planets and moons (e.g. [174, 159, 144, 17, 114, 74]) and for flows around comets ([55, 56]).

The solar wind is most often high-β and the solar wind Mach number is high ($M \sim 10$), such that pressure effects dominate over magnetic effects. The magnetically dominated parameter regime for which we do find the complex bow shock topology of Fig. 2.8b, is thus not typical for the solar wind. This explains probably why this parameter regime — to our best knowledge — has not been considered before in 3D MHD simulations of terrestrial bow shock flows [174, 16]. However, we explain further on that the solar wind can be magnetically dominated at the earth for up to 8% of the time. This means that the earth's bow shock flow may exhibit the complex topology with the secondary slow shock of Fig. 2.8b under those magnetically dominated solar wind conditions. Some satellite observations do indeed suggest that a slow shock may be

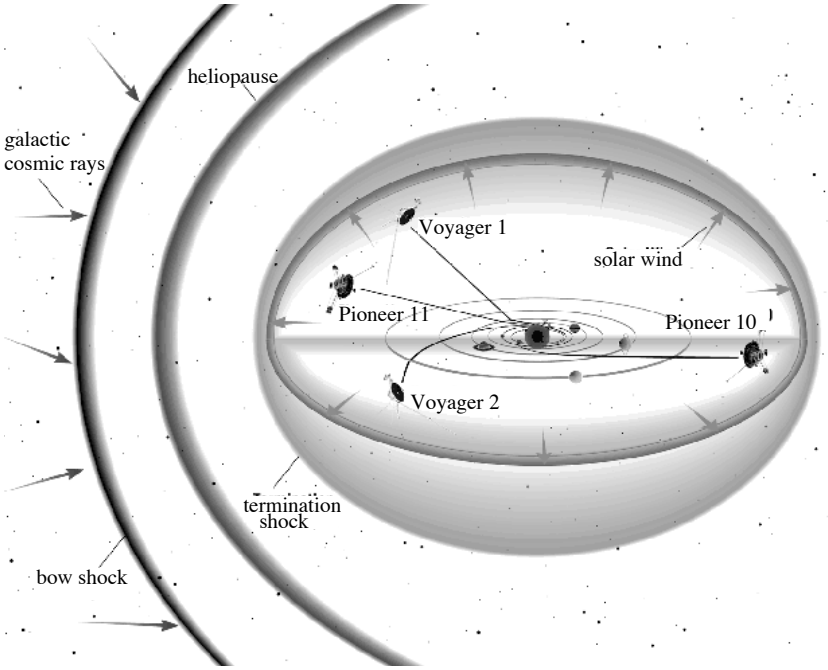

Figure 2.11: *The solar system's magnetic environment or* heliosphere. *The sun is located in the center of the picture. (courtesy NASA)*

found in the earth's magnetosheath downstream of the bow shock [141]. Our simulation results exhibit such secondary shock fronts of slow type following the leading bow shock, and the observed slow secondary shock in the earth's magnetosheath may be due to a process similar to what is described in our simulations. In particular, our 3D simulation results of Fig. 2.8b suggest that such a secondary shock front should be present only on one side of the sun-earth line. It would be interesting to verify this in the earth's magnetosheath using observations by several satellites covering different locations in the global system. The application of our simulation results to the earth's bow shock flow is discussed in detail in Chap. 8.

It is believed that a superfast interstellar wind interacts with the whole solar system to produce a *heliospheric* magnetic configuration [64] like the one sketched in Fig. 2.11. A heliospheric bow shock is expected to exist. Fig. 2.11 also shows the approximate trajectories of several spacecraft that were launched to study the solar system. The heliospheric magnetic configuration has been modeled using MHD (e.g.

[117, 124, 100]), and it is expected that observational tests for these models will become available when several outward traveling spacecraft will cross the heliospheric termination shock (Fig. 2.11) early in the 21st century. Not much is known about the conditions in the interstellar wind, so it is an open question whether the flow upstream of the heliospheric bow shock can be magnetically dominated.

2.3.4 Solar coronal mass ejections and traveling interplanetary shocks

Up to several times per day, large-scale structures in the solar corona disrupt and are ejected out of the corona at speeds ranging from 10 to 2×10^3 km s^{-1}, carrying a mass of 10^{12-13} kg and liberating an energy of 10^{24-25} J [66, 104, 68]. Many aspects of the propagation of coronal mass ejections (CMEs) in the solar coronal plasma can be described by the equations of ideal MHD. White light coronagraph observations of fast CMEs show bright leading fronts which can be interpreted as signatures of fast MHD shock fronts [68].

Fig. 2.12 shows two consecutive images taken by the SMM coronagraph, on 30 January 1989, at 2:11 and 2:28 UT. A bright spiraling prominence structure is seen to expand rapidly, and is preceded by a bright loop-like structure. This leading front contains a small 'dimple' in the image on the left. In the right image, about 17 minutes later, the leading front is less bright, but the dimple is more pronounced, and the leading front seems to be followed by secondary fronts. The plasma β in the inner solar corona is believed to be substantially smaller than unity, and the fast MHD wave speed is believed to be of the order of 600 km/s. The projected velocity of the leading front in Fig. 2.12 is 1055 km/s. These numbers indicate that the flow upstream of the leading shock front may well be magnetically dominated. Steinolfson and Hundhausen [147, 146] studied these dimpled leading fronts, they related the dimple to the properties of switch-on shocks, and they performed time-dependent numerical MHD simulations in 2D. Their simulations of moving shock fronts confirmed the existence of the dimple effect, and seemed to contain intermediate shocks.

Steinolfson and Hundhausen's work was the motivation and starting point for the work described in this dissertation. We study the formation of MHD shocks with magnetically dominated upstream flow, not in a time-dependent outflow driven by a pressure pulse as in Steinolfson and Hundhausen's case, but in the much simpler setting of a uniform flow falling in on a perfectly conducting cylinder or sphere. This simple setting allows us to analyze the stationary flow results in a rigorous way. It allows us to describe the intricate secondary shock patterns discovered in our simulation results and not anticipated by Steinolfson and Hund-

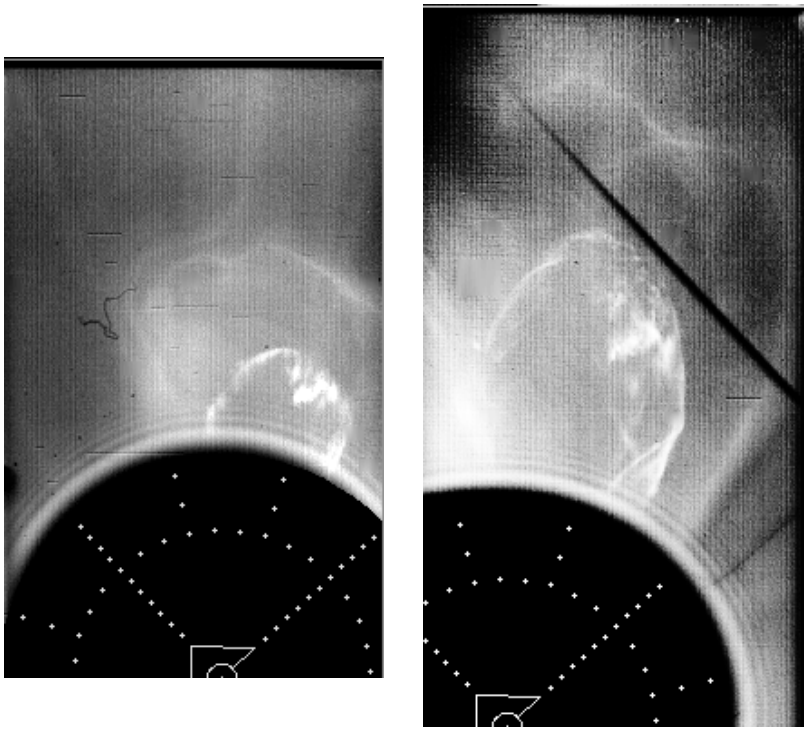

Figure 2.12: *SMM coronagraph images of a CME. The sun is blacked out by a disc with radius* 1.6 R_{sun}.

hausen's important earlier work, and to identify clearly intermediate and compound shocks. In Chap. 8 we discuss how our simulation results are relevant for shocks induced by fast CMEs.

It is believed that the shocks induced by fast CMEs propagate through the interplanetary space as interplanetary shocks [136]. They may travel in the direction of the earth as the leading edges of magnetic clouds [15, 58]. Magnetic clouds often cause magnetic storms, which are severe disruptions of the earth's magnetic environment, disturbing communications and sometimes even leading to power failures. Fig. 2.13 shows measurements by the WIND satellite, which is located in front of the earth's bow shock. Discontinuous jumps in magnetic field, ion density, and ion temperature, indicate the arrival of interplanetary shocks [58]. The magnetic effects on bow shock topology discovered in our simulation results may also become important when magnetic clouds reach the earth's bow shock, because the magnetic field is strong in magnetic clouds. We speculate in Chap. 8 that intrinsically magnetic effects may

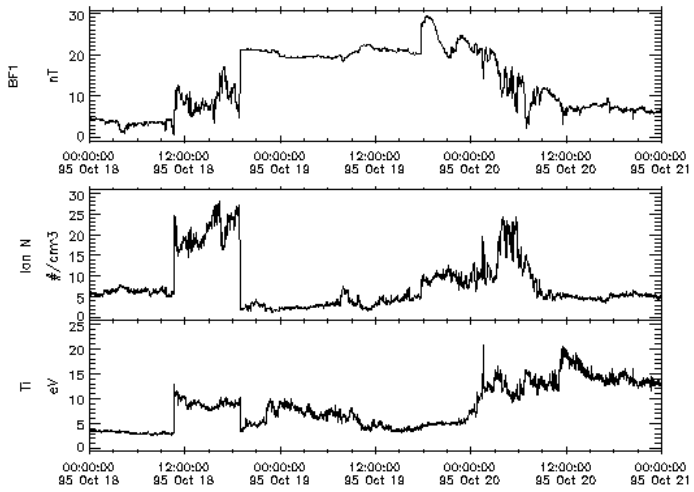

Figure 2.13: *Interplanetary shock just before it reaches the Earth's magnetic system. (WIND satellite data, courtesy R. Lin and R. Lepping, CDAWEB)*

cause a global reconfiguration of the magnetosheath flow which may determine the timing of magnetic storm onset.

An important application of space physics and solar physics is the study of 'space weather', which is concerned with disturbances of the earth's magnetic system by perturbations in the solar wind. Those perturbations are believed to originate directly on the sun. The ultimate goal is to provide operational predicting capabilities, much like weather prediction on earth, which could help in reducing the harmful effects of magnetic storms. One of the possible approaches to this problem is the global simulation of the sun-earth system, and for this the MHD model seems to offer a physical starting point that promises both accuracy and tractability. Much can be learned from problems with reduced complexity, like the stationary bow shock flows discussed in this dissertation. This knowledge then serves as a part of the intuitive basis to understand the simulation of more complex systems comprising the time-dependent evolution of magnetic disturbances originating at the sun, propagating through the solar wind, and interacting with the quasi-stationary bow shock and magnetosphere of the earth. This is an ambitious program, but first attempts are made using adaptive grids to cover the different spatial scales, and the resulting MHD models are capable of delivering faster-than-real-time turn-around on the world's largest supercomputers.

The problems faced in trying to understand these complicated in-

teractions are obviously enormous, and as is not unusual for ambitious undertakings, the space weather project meets with a lot of criticism from many established scientists, especially about the operational aspect. Of the many points of criticism, we can mention the following two. It is argued that many essential physical processes — including the heating mechanism of the solar corona — are not understood, and that numerical methods cannot make deterministic predictions about nonlinear physical systems which may involve chaotic behavior. We believe that space weather prediction is indeed an extremely difficult task, but we are not convinced that there are solid theoretical arguments which would indicate that the prediction of space weather is fundamentally impossible. Indeed, physical processes of which the microscopic mechanisms are not well known, can be incorporated into large-scale models in a parametrized way. A good example is the relatively successful parametrization of turbulence in gasdynamic or atmospheric physics applications [167, 101]. The detection at the earth of magnetic clouds as well-structured entities with components which can directly be related to pre-CME structures in the lower solar corona [15, 58], shows that space weather events may be caused by deterministic large-scale flow patterns, and may not be influenced too much by perturbations of a chaotic nature.

We believe that the problems which can be addressed in large-scale MHD simulations of the sun-earth system are interesting and important, and next to the operational and predictional aspects, a lot has to be learned regarding the complex interaction of nonlinear phenomena in three space dimensions. We think that global MHD simulations are a good way to approach these complex interactions. It is our belief that global time-dependent MHD simulations will indeed become more and more feasible and that much can be learned from them, and we do see the results of this dissertation and the methods employed as an initial step towards such a goal.

2.3.5 Astrophysical shock phenomena

Magnetic fields are believed to play an important role in many astrophysical phenomena. Since the launch of the Hubble Space Telescope (HST), observations become available with sufficient resolution for the direct observation of shock phenomena in distant astrophysical objects. Fig. 2.14 shows HST images of jets emanating from young stellar objects. Magnetic fields are believed to be important for the collimation of these jets, and shocks are observed at the leading edges of the jets [29, 126]. Many MHD simulations have been performed on the subject of astrophysical jets [165], and it is argued that some complex morphological characteristics of those objects can be explained using MHD models.

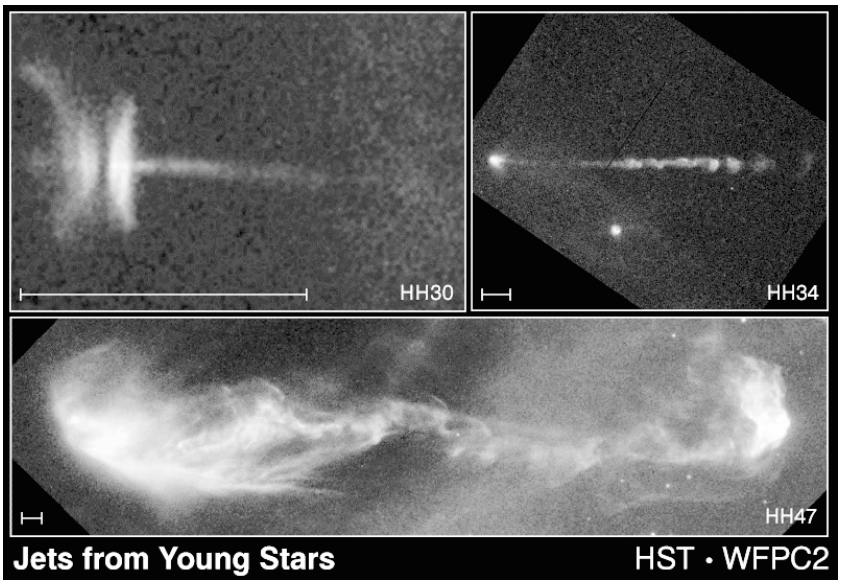

Figure 2.14: *Jets from young stellar objects. It is believed that during star formation stellar outflow is collimated into bipolar jets perpendicular to an accretion disk. In the bottom image, for instance (HH47), a large horizontally extended jet is seen. The jet induces a bow shock on the leading edge (far right), and several additional bow shocks and internal shocks have been identified [126]. (courtesy C. Burrows, J. Hester, and J. Morse, NASA)*

MHD models are employed for the study of shock phenomena in various other astrophysical objects, like jets ejected from active galactic nuclei [166] and the interaction of supernova remnants with the interstellar medium [25]. General relativistic MHD equations are used to study the formation of shock waves in magnetohydrodynamical accretion onto a black hole [181].

The use of magnetic fields in the study of astrophysical objects is, however, still relatively new and unexplored, and the magnetically dominated bow shock flows which are described in this dissertation may have applications in astrophysical flows when upstream plasmas are magnetically dominated.

2.3.6 Laboratory plasmas and magnetic reconnection

Plasmas have been studied intensively in the laboratory. MHD shocks have been studied in plasma shock tubes [4, 92]. Models of the earth's magnetic system are being studied in the laboratory, where an intense plasma flow simulating the solar wind interacts with a magnetized 'terrella' [123], resulting in a flow with a bow shock and a magnetosphere. Spacecraft re-entry is simulated in plasma wind tunnels or plasmatrons [9], where a sample is exposed to a supersonic partially-ionized plasma, resulting in a flow with a bow shock.

In the last decades much effort has been devoted to the study of controlled nuclear fusion, mainly in tokamak devices. Tokamak plasmas can be described approximatively by the MHD equations. Linear MHD stability calculations impose important bounds on tokamak stability limits [116]. The numerical MHD code described in this dissertation has been used to describe the dynamics of hot filaments in a tokamak plasma. Because it does not deal directly with MHD shock phenomena, this work is not described in this dissertation, but is reported elsewhere [155]. MHD shock phenomena are not studied so much in the context of tokamak physics, probably because shocks are generally believed to be related to disruption of the plasma, which one tries to avoid. It remains difficult to measure densities and magnetic fields inside tokamak plasmas, such that it is hard to know if, when and where shocks would be formed.

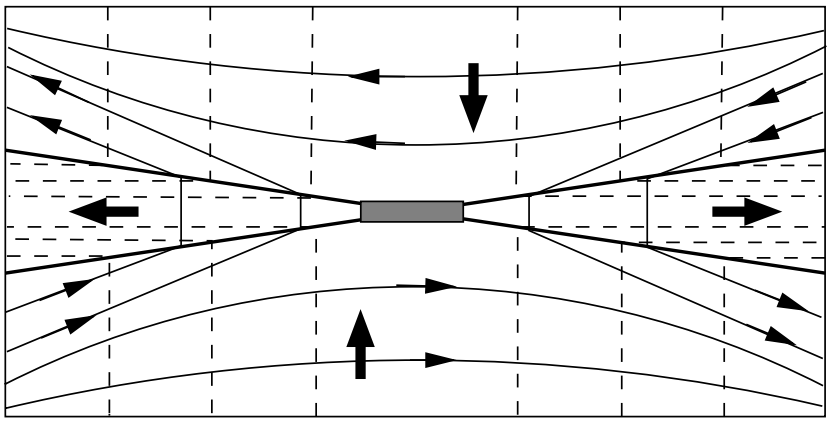

Figure 2.15: *Topology of the Petschek reconnection model. Magnetic field lines (thin solid) and streamlines (dashed) are refracted at slow shocks (thick solid). Reconnection takes place in the central shaded diffusive region.*

The process of *magnetic reconnection* is another subject of active theoretical study [86, 39, 119, 8]. Magnetic reconnection can naively be depicted as the process in which a region of plasma changes its magnetic topology by breaking magnetic field lines and connecting the broken ends to other broken field lines as the result of electrical resistivity. Magnetic reconnection is an inherently resistive process, and in highly conductive plasmas it is in general restricted to small regions where gradients of the magnetic field (and thus currents) become very large. Fig. 2.15 shows a sketch of a popular reconnection mechanism proposed by Petschek in 1963 in which shocks play an intrinsic role. Plasma is brought in from above and below, and is deflected towards the left and the right by slow MHD shocks. In a small central region the gradients of the magnetic field become very large and reconnection takes place. This is only one theoretical model of MHD reconnection, and it has not been proven that it actually works in practice [86]. Other reconnection models, however, also contain MHD shocks, and it has even been argued that the existence of intermediate MHD shocks is essential for reconnection [96]. Magnetic reconnection for plasmas in the MHD regime has recently been studied in laboratory experiments [179, 72]. Some numerical MHD simulations seem to confirm the importance of MHD shocks for reconnection phenomena [39, 132], but there is still much discussion about the true nature of MHD reconnection, and much of the numerical results seem to be critically dependent on the formulation of the boundary conditions [39, 8].

Magnetic reconnection is also believed to be an important process in many solar and space plasmas, and many numerical simulations are performed which attempt to describe this. Solar corona X-ray jets were modeled using the resistive MHD equations, and fast MHD shocks occur at the reconnection site [182]. Reconnection is believed to be important at the earth's magnetopause and magnetotail, and many numerical simulations have been performed using MHD models [133, 94, 96, 175]. The simulation results have been compared with the abundant observational data available from satellite magnetopause crossings. Recently hybrid simulations have been performed, where the electrons are treated as a massless fluid and the ions are treated as particles, and the results from these simulations seem able to explain some of the wave features present in the observations but not described by MHD [89, 176, 78, 76, 77, 95, 98, 134, 112]. These simulations are certainly a step beyond MHD simulations and may explain additional physical phenomena, but it seems that much care has to be exercised in evaluating the numerical results, because a unique closure is not available for the hybrid system, because its mathematical properties are not well-known, and because only numerical results are available. For instance, the influence of the formulation of the boundary conditions may even be more important than in the MHD case [39].

2.4 Analytical and numerical techniques to study MHD shock phenomena

An important part of this dissertation deals with analytical and numerical techniques to study MHD shock phenomena. Much of the knowledge necessary in this study did only partially exist and had to be collected and developed as a large part of the thesis work.

The main analytical technique used in this dissertation to analyze steady state MHD flows in 2D is the theory of stationary characteristics. This theory also turns out to be useful for the validation of numerical results. An extensive general theory exists for the characteristic properties of symmetric hyperbolic systems [21, 20]. This theory has been applied early on to unsteady MHD flows [21] and to steady MHD flows, including the case where the magnetic field is aligned with the flow (field-aligned or parallel flow) [79, 59]. More complete accounts of the characteristic theory of steady and unsteady MHD flows appeared later [71, 85, 70, 3]. In Chap. 3 we present a new derivation of this characteristic theory, based on the Galilean invariant symmetrizable form of the conservative MHD equations [52, 118, 7] with a source term (the right hand side term proportional to $\nabla \cdot \vec{B}$ in Eq. 2.6) and using a matrix approach [70, 19]. This derivation gives insight into the structure of the MHD equations as a system of Galilean invariant conservation laws with a constraint, and in a simple, compact, and systematic way we recover all the various results that are scattered throughout the literature.

Numerical simulations of MHD flows with shocks have been performed for many decades, but most of the time relatively primitive numerical techniques of Lax-Wendroff or Flux Corrected Transport type were used. Numerical codes typically either were excessively diffusive or produced spurious oscillations near discontinuities. In the mean time robust and accurate shock-capturing numerical techniques of the so-called high-resolution type were developed in the domain of Computational Fluid Dynamics (CFD) [90]. Only since a decade or so, some of these new numerical methods have started to be used in MHD codes. The MHD system has a few peculiar properties which impeded the straight translation of the CFD techniques, but it seems that the main obstacles have been cleared in recent work by Roe and Balsara (1996) [127], who provided a well-behaved eigensystem decomposition of the MHD Jacobian, and by Powell (1995) [118], who provided a consistent and efficient way to deal numerically with the $\nabla \cdot \vec{B} = 0$ constraint via a source term (the right hand side term proportional to $\nabla \cdot \vec{B}$ in Eq. 2.6). In Chap. 4 of this dissertation we report on the development of the massively parallel shock capturing MHD code PAR-MA (PARallel MAgnetohydrodynamics). Starting from the proven CFD concepts present in the von Karman

institute multi-block solver [106], and incorporating the essential contributions of Roe and Powell [1], a robust and accurate high-resolution MHD flow solver was developed. Numerical techniques similar to the one used in this dissertation are currently being used in several application codes [118, 162, 124, 117], but not much can be found in the literature about rigorous validation of this approach. In Chap. 5 it is shown through careful validation studies based on characteristic theory that the from CFD derived numerical MHD scheme produces valid results.